Flow in complex terrain - a Large Eddy Simulation comparison study

Berg, J.; Troldborg, Niels; Menke, Robert; Patton, E. G.; Sullivan, P. P.; Mann, Jakob; Sørensen, N.N.

Published in:
Journal of Physics: Conference Series

Link to article, DOI:
10.1088/1742-6596/1037/7/072015

Publication date:
2018

Document Version
Publisher's PDF, also known as Version of record

Flow in complex terrain - a Large Eddy Simulation comparison study

IOP Conf. Series: Journal of Physics: Conf. Series **1037** (2018) 072015 doi:10.1088/1742-6596/1037/7/072015

Flow in complex terrain - a Large Eddy Simulation comparison study

J. Berg[1], N. Troldborg[1], R. Menke[1], E. G. Patton[2], P. P. Sullivan[2], J. Mann[1] and N.N. Sørensen[1]

[1]DTU Wind Energy, Frederiksborgvej 399, 4000 Roskilde, Denmark jbej@dtu.dk
[2] National Center for Atmospheric Research, Boulder, CO, US.

E-mail: jbej@dtu.dk

Abstract. We present Large-Eddy Simulation (LES) results of flow over the double ridge complex site at Perdigão in Portugal. The focus is to compare simulated flow features from two LES codes with different discretization techniques. We compare a finite volume discretization with a pseudo spectral approach in two different terrains. Mean wind properties and turbulent kinetic energy from the two codes are to a large degree in agreement. The largest discrepancy we observe is attributed to the different effective resolution in the two codes which results from the numerical discretizations. Comparison with measured data from three installed meteorological masts inside the simulated domain show that many of the main flow features have been captured by the LES simulations despite its relatively simple setup.

1. Introduction

Modelling of flow in complex terrain is both a scientific challenge as well as an important task when it comes to siting of onshore wind turbines. With the Askervein Experiment in the 80ies [24, 27] the wind modelling community for the first time got a well chosen and carried out reference case to use for validation for wind modeling. The focus of the Askervein campaign with its relatively gentle slopes was linearised solvers as those of the Jackson-Hunt type [6] including the WAsP suite used in the first European Wind Atlas [25]. Another landmark was the Bolund campaign carried out in 2007-2008 [2, 1]. The steep and almost vertical cliff at Bolund in the main wind direction was a big challenge for the models and both RANS and LES models had difficulties capturing the high turbulence level on the top and behind the hill. The small size of Bolund, however, made the influence of atmospheric stratification and Coriolis force negligible and therefore not ideal for real siting applications, although important lessons of flow in complex terrain can still be learned [4, 8, 9].

The large scale double ridge at Perdigão in Portugal is on of the latest additions to the suite of orography reference cases. The main measurement campaign ended in 2017 (a few meteorological masts are still in operation) and is part of a larger international measurement campaign series under the EU New European Wind Atlas Project [10, 26].

The whole point of using LES compared to RANS is the inclusion of non-stationary flow features and a detailed picture of the turbulent kinetic energy by scale. Both are objectives which are necessary for accurate estimation of wind turbine loads through actuator disk and line methodologies. A previous study [3] with a setup similar to one of the flow cases studied in this paper, analyzed the influence of complex terrain upon the behaviour of wind turbine wakes.

In this contribution we will use the site of Perdigão as reference case and perform multiple LES simulations with two different model types. We will present a comparison between the NCAR pseudo spectral model [21, 23] (ps-NCAR) and the finite volume code EllipSys3D [17]. To successfully simulate the various flow configurations at Perdigão the inclusion of both atmospheric stratification and Coriolis force will be needed as well as terrain details and land surface usage in a large area surrounding the site. In this paper, we will, however, confine the analysis to strictly neutral stratification (enforced constant pressure gradient balanced by form drag and surface momentum flux, i.e. no Coriolis force) in order to address the differences which might occur due to different numerical discretizations procedures - pseudo spectral versus finite volume. Also the roughness description is kept simple and the extent of the domain is limited. The focus of the paper is therefore to compare the two types of LES models and not to necessarily match a given set of measurements. Since measurements are available, we do, however, present a comparison and list a number of factors which makes such a comparison imperfect.

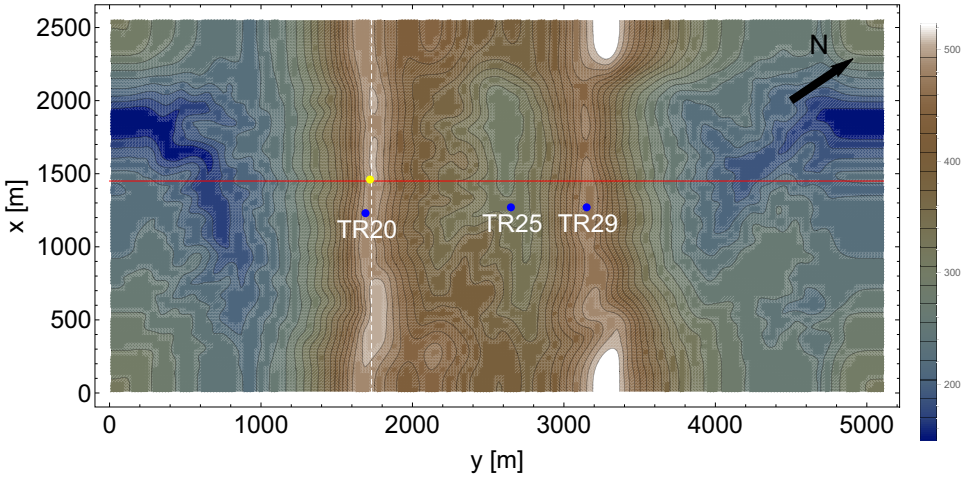

Figure 1: Perdigão terrain heights. The main transect studied in this paper is the red line and the white line indicates the SW ridge. The meteorological masts are shown with blue dots.

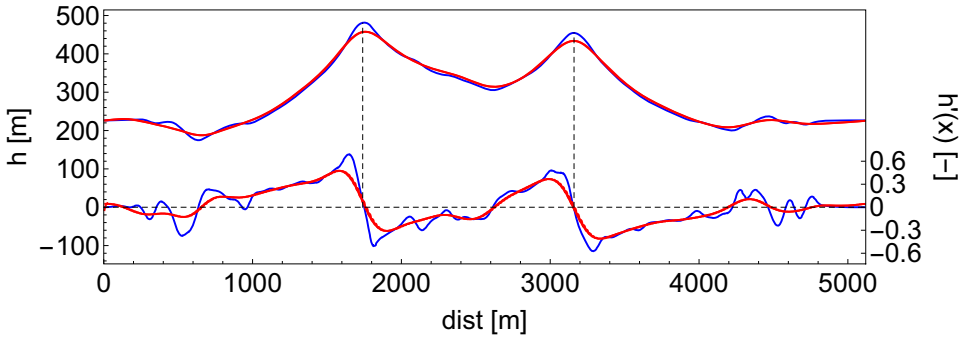

Figure 2: Terrain height, $h(x)$, and slope, $h'(x)$, along the the main transect for steep (*blue lines*) and smooth (*red lines*) terrain files of Perdigão.

2. LES setup

Both EllipSys3D and ps-NCAR are run on the same terrain surface files with similar horizontal grid spacing. Three surface files are used: 1) a steep terrain file with a horizontal resolution of 20 m, which resembles the real topography. 2) a smoothed terrain file with a horizontal resolution of 20 m, similar to the one used in [3]. 3) A 10 m, resolution version of 2). It should be noted that the vertical discretization is the same as in 2) meaning that the aspect ratio, $\Delta x/\Delta z$, is changed by a factor of two. The terrain smoothing was performed in Fourier space by multiplying the individual Fourier modes, $\hat{h}(k_x, k_y)$, by $\exp\left(-4((k_x\Delta x)^2 + (k_y\Delta y)^2)\right)$.

For all three terrain cases the domain size is $5120 \times 2560 \times 3000$ m^3. The steep terrain is presented in Figure 1. The two ridges are clearly visible with an orientation 90° to the incoming wind direction which is along the x-axis. The main transect (red line) is plotted in Figure 2 and compared to its smoothed version. Both the maximum slope located at the first ridge and small-scale variations are much higher in the steep non-smoothed version. The findings in [9] suggest that such orographic changes could have dramatic consequences for the flow field.

The driving pressure gradient is held constant throughout the study at $dP/dx = -u_\tau^2/H$, where $u_\tau = 0.6\,\mathrm{m\ s}^1$ and $H = 3000$ m is the height of the computational domain (for comparison the lowest terrain height is located at 150 m) With constant roughness length, $z_0 = 0.5$ m, we have $z_0/H = 1.67 \times 10^{-4}$. The simulations ran for a large number of large eddy turn-over times until stationarity was reached and we could start sampling. Stationarity was here defined as a constant area averaged surface momentum flux over time. As we will see later such a definition might not be applicable in all situations.

Statistics has been gathered from 30-min averages. We have collected rather large ensembles in order also to estimate the model variability present on time scales longer than 30 minutes. The number of averages analyzed, N_{30min}, together with other key features of the simulations can be found in Table 1.

Table 1: LES simulations

Name	Terrain	Grid points	Δx [m]	N_{30min} [−]	U_{norm} [m s^{-1}]
EllipSys3D	steep	$256 \times 128 \times 128$	20	55	3.16
EllipSys3D	smooth	$256 \times 128 \times 128$	20	101	3.76
EllipSys3D	smooth	$512 \times 256 \times 128$	10	43	3.71
ps-NCAR	steep	$256 \times 128 \times 128$	20	50	2.84
ps-NCAR	smooth	$256 \times 128 \times 128$	20	58	3.43
ps-NCAR	smooth	$512 \times 256 \times 128$	10	24	4.03

The domain is periodic in both horizontal directions and both models use periodic boundary conditions in the horizontal directions. Both models also use the one-equation Deardorff Sub-Grid Scale (SGS) model [13, 20, 21] and apply a stress free (zero shear and $w = 0$) top boundary condition.

The simulations are driven with the same constant pressure gradient. Small differences in the strength of the flow from the two models are, however, observed, and could be due to the different ways we implement the lower boundary condition and generate the mesh (see below). In the analysis all results are as a consequence non-dimensionalized with the average streamwise wind speed at position, $x = 30$ m, and $z = 80$ m denoted by U_{norm} in Table 1. The slightly higher value of ps-NCAR 10 m resolution could be due to the fact that stationarity of all scales has not yet been fully reached in the simulation.

An important finding is the relative difference in the strength of the flow as quantified by U_{norm} in the steep and smooth cases. For both LES models U_{norm} is 19% higher in the smooth case compared to the steep case.

Differences in the two models are described in the following subsections:

2.1. EllipSys3D

EllipSys3D [11, 12, 17] solves finite volume discretized incompressible Navier-Stokes equations in general curvilinear coordinates. EllipSys3D uses a collocated grid arrangement and Rhie-Chow interpolation is used to avoid pressure-velocity decoupling. The solution is advanced in time using a second-order iterative time-stepping method. In the present work the coupled momentum and pressure-correction equations are solved using the semi-implicit method for pressure linked equations (SIMPLE)[16], and the convective terms are discretized with a fourth order accurate central difference scheme. When running in LES mode, EllipSys3D solves the filtered incompressible Navier-Stokes equations using an implicit filter, where only the filter width is specified. In the present work the filter width is set to $vol^{1/3}$, where vol is the volume of a cell while the time step is set to 0.5 s.

Neutral surface layer scaling is enforced at each point at the lower grid level. In the formulation $z = 0$ is placed on top of z_0, which mean that cells with an infinitely low height can be used close to the surface.

Two different methods are used to construct a volume mesh for a given ground surface mesh: one where grid cells are grown vertically away from the ground and one where cells are grown away using HypGrid [18]. The latter approach ensures more orthogonal cells which should enhance convergence, but on the other hand this method also produces a horizontal expansion of convex grid regions and contraction of concave regions and hence coarser resolution. See the right panel of Figure 3 for a illustration of the two meshes. In the left panel we show a comparison of the streamwise velocity component 40 m above terrain along the main transect as depicted in Figure 1. The velocities are very similar (we have also looked at 80 and 120 m above terrain), so from now on we only use the mesh with vertical lines due to its resemblance to the one used with the ps-NCAR code, which will be presented in the next subsection. It should, however, be noted that more careful investigations need to be carried out before more conclusive statements can be made.

The model is driven by a constant body force corresponding to a constant pressure gradient.

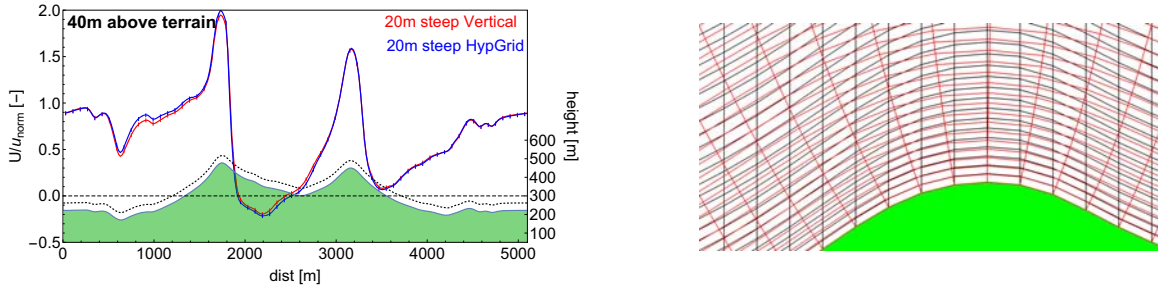

Figure 3: *Left:* Transect plot of mean streamwise velocity for EllipSys3D with two different mesh types; vertical and HypGrid *Right:* Sketch of meshes with vertical growth from surface (*black lines*) and with HypGrid (*red lines*). No resemblance with actual aspect ratios in our simulations.

2.2. ps-NCAR

The LES code is developed for a spectrum of moving waves in the marine atmospheric boundary layer [21], and an early version of the code was used for studying generic properties of flow around hills and gap flows [23]. It is a pseudo-spectral code; wave number representation in the two horizontal directions and central second order finite differencing in the vertical direction. The

Boussinesq approximation is adopted and the governing equations are integrated forward in time using adaptive time stepping (in the current simulations, Δt varied between 0.74 s and 0.78 s in the steep case) in a terrain following coordinate system: whereas the horizontal coordinate lines are Cartesian the vertical coordinate, z, is related to a terrain following ζ-coordinate (in which the LES equations are cast) and the local terrain height, h, according to the rule $z(x, y) = \zeta + h(x, y)(1 - \zeta/H)$, z is chosen exponential stretched away from the surface.

The pressure is solved during an iterative procedure of a general Poisson equation with a strong coupling between w and p. Details of the coupling and the usage of local contravariantflux velocity variables are fully described in [21]. Compared to running the model on flat terrain [22] this last step slows down the code substantially, especially in very steep terrain as encountered in this study: we used approximately twice as many iteration steps in the steep case compared to the smooth cases.

Due to the the spectral representation in the horizontal directions the top 1/3 wave-numbers have been cut-off in order to avoid aliasing effects. This means that the effective resolution in the NCAR simulations are a factor, $(3/2 \times 3/2 \times 1)^{1/3} \sim 1.31$, lower compared to the EllipSys3D simulations, which on the other hand do not have a clear cut-of due to implicit filtering. As we will see later this has consequences on the amount of SGS vs resolved turbulent kinetic energy produced.

Neutral surface layer scaling is enforced at each point at the lower grid level like with Ellipsys3D. z_0 is however contained inside the first cell, which mean that $z_1 >> z_0$. We have $z_1 \sim 2.5$ m (the height at the center of the lowest grid cell). This aspect ratio of 4 is on the border of recommended usage.

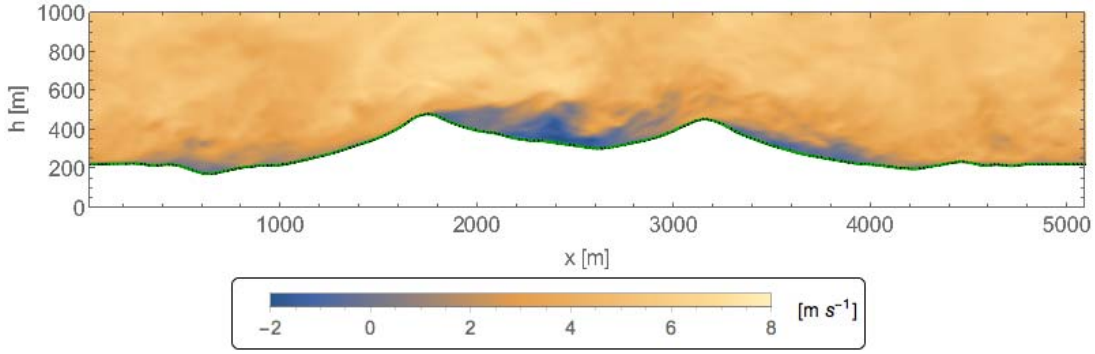

Figure 4: Snapshot of streamwise velocity, u, along the main transect with ps-NCAR in the steep case.

3. Results

We use the following notation: $\langle\cdot\rangle$ denotes ensemble averaging and $\overline{(\cdot)}$ denote 30-min time averaging of resolved velocity components, $u_i(\mathbf{x}, t)$, and their fluctuations in time, $u_i'(\mathbf{x}, t) = u_i(\mathbf{x}, t) - \overline{u_i(\mathbf{x}, \mathbf{t})}$. Mean streamwise velocity is constructed as $U = \langle\overline{u_1}\rangle$, 3D wind speed as $S = \left\langle\overline{\sqrt{u_i u_i}}\right\rangle$, resolved turbulent kinetic energy as $\frac{1}{2}\left\langle\overline{u_i' u_i'}\right\rangle$, and total turbulent kinetic energy as $TKE = \left\langle\frac{1}{2}\overline{u_i' u_i'} + \overline{e}\right\rangle$, where e is the SGS turbulent kinetic energy.

3.1. Model to model transect comparison

A snapshot of the instantaneous velocity in the x direction, U is presented in Figure 4. Strong recirculation zones are evident behind both ridges. Focusing on the flow at typical wind turbine hub heights we present wind speed and turbulent kinetic energy along the main transect

presented in Figure 1 at heights, 40, 80 and 120 m above terrain. The wind speeds, U/U_{norm}, are presented in the left panels of Figure 5 - 7 while the corresponding total kinetic energies, TKE/U^2_{norm} are presented in the right panels. For the wind speeds the two models EllipSys3D (full lines) and ps-NCAR (dashed lines) in general agree well. For the 20 m resolution smooth case the agreement is close to striking with collapsing curves (within errorbars) for all heights and x positions. Only in between the two ridges, the valley region, do we observe small differences in the 40 and 80 m height plots. For the 10 m resolution the two codes show opposite tendencies in the valley region. Whereas EllipSys3D show less reduction ps-NCAR code show more. On the ridges the two smooth EllipSys3D run coincide. We thus as, already mention, conclude that the 10 m resolution ps-NCAR run is not fully converged. The conclusion on mean wind speed in the smoothed runs is therefore that speed-up on the two ridges is captured with 20 m resolution while reduction in the valley is not. For the steep runs ps-NCAR show more reduction in the valley region while the speed-up on the ridges is somewhat smaller. The recovery after the second ridge is similar for the two models.

For the turbulent kinetic energy there is naturally much more variation between the two models and in between the different flow cases. Upstream (which due to the periodic boundary conditions in principle also is far behind the ridges) EllipSys3D has a higher level of TKE/U^2_{norm} compared to ps-NCAR. For both 20 m cases the level at the first ridge, in the valley region and at the second ridge, is on the other hand, very similar for the models. Especially in the smooth case the agreement is very convincing. The picture from 10 m resolution runs show a more complex pattern. The main trend though seems to be a higher level right after the first ridge and a lower level in the upstream region.

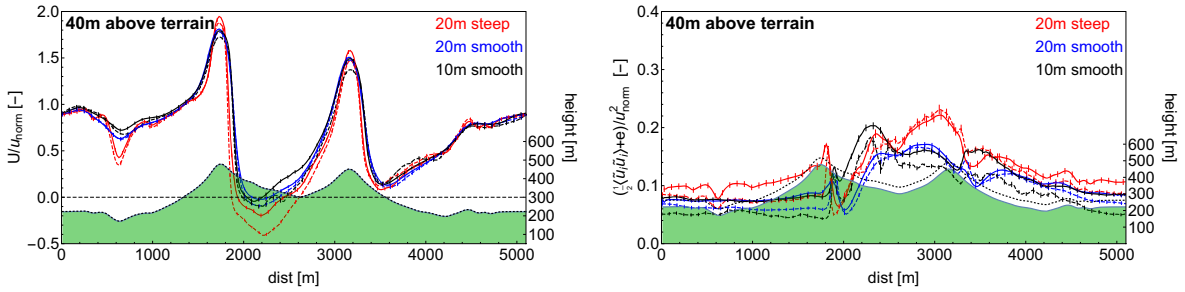

Figure 5: Main transect at 40 m height above the terrain. *Left:* Non-dimensionalized mean streamwise velocity, U/U_{norm}. *Right:* Non-dimensionalized resolved turbulent kinetic energy, TKE/U^2_{norm}. EllipSys3D (*full lines*) and ps-NCAR (*dashed lines*)

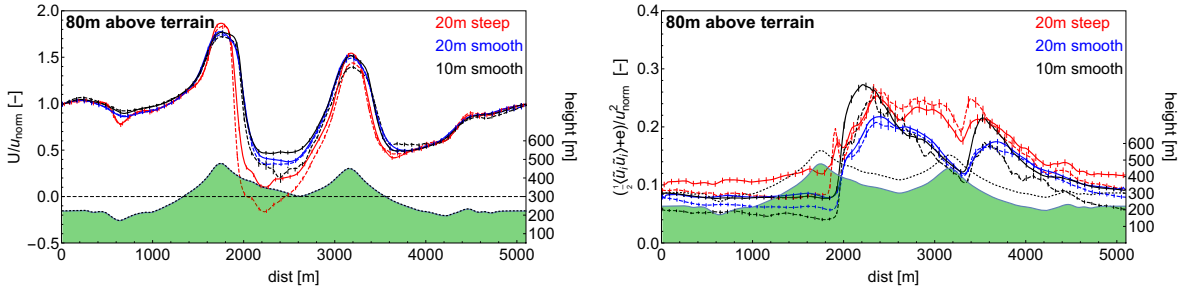

Figure 6: same as Figure 5 but for 80 m.

As a last thing we look in Figure 8 at the ratio between SGS and resolved turbulent kinetic energy. Due to a lower effective resolution in the ps-NCAR codes as previously discussed we find

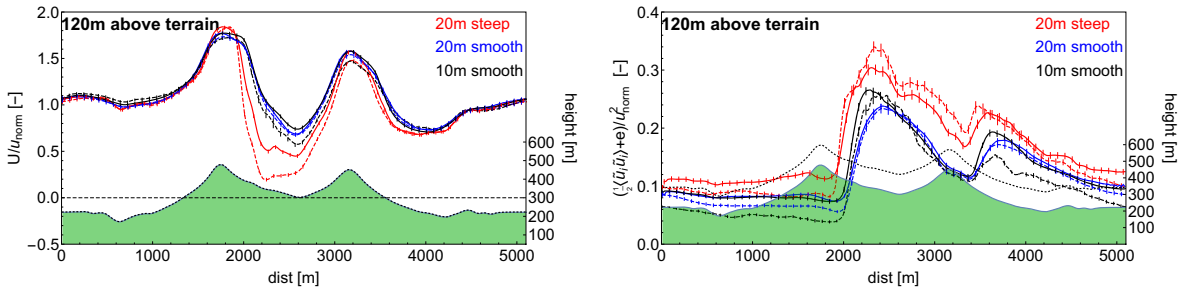

Figure 7: same as Figure 5 but for 120 m.

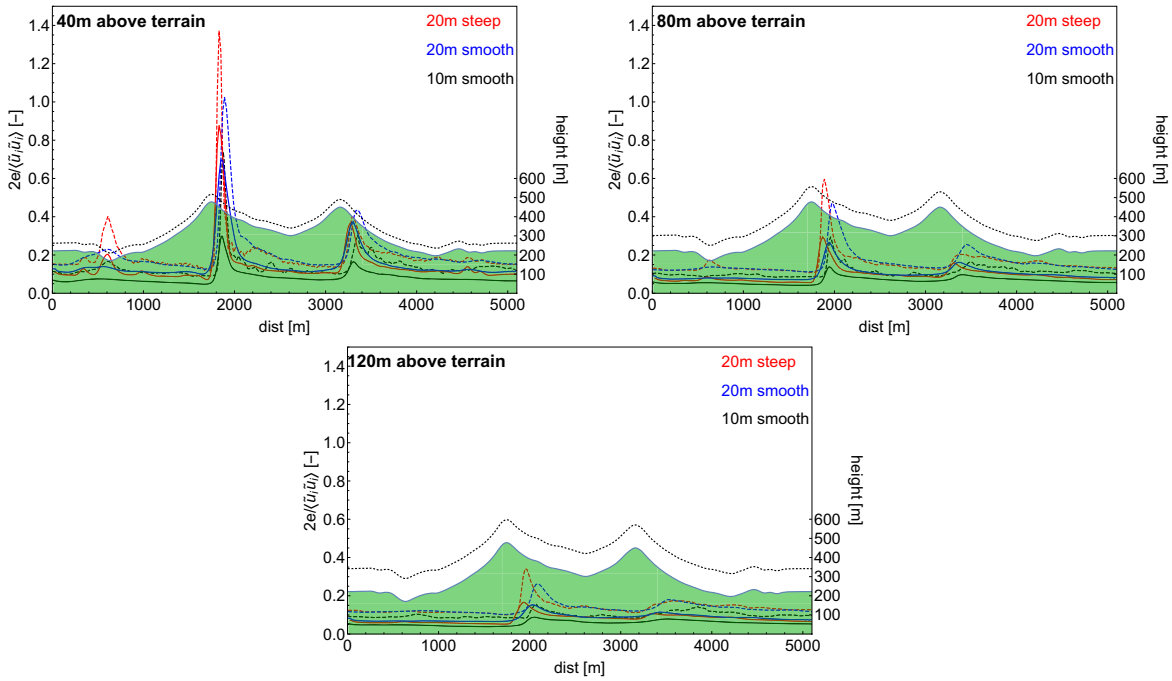

Figure 8: Main transect at 40, 80 and 120 m height above the terrain. Ratio between e, and resolved turbulent kinetic energy, $\frac{1}{2}\langle\widetilde{u}_i\widetilde{u}_i\rangle$. EllipSys3D (*full lines*) and ps-NCAR (*dashed lines*)

a higher ratio for all x positions and heights. At the first rige the ratio is more than one meaning that the LES ansatz breaks. However, it is important to mention that the lower ratio found for EllipSys3D only means that a larger percentage of the flow is resolved. Due to the implicit filter in EllipSys3D the extra resolved turbulence close to the filter size might in principle be due to non-physical behavior, i.e. a consequence of the numerics and not the physical flow properties. We therefore can not say whether EllipSys3D resolves more of the terrain induced turbulent kinetic energy.

An interesting question is whether the periodic boundary conditions enforced here together with the domain length of 5120 m affect the flow in way that the inflow to the first ridge is directly influenced by the second ridge. Future studies with added buffer regions of various sizes as well as fringe regions [19, 14, 15] will show whether this is true.

3.2. Model to measurements profile comparison

We compare the steep cases from both EllipSys3D and ps-NCAR with measurements from sonics installed on three meteorological masts. The three masts, TR20, TR25 and TR29, are indicated

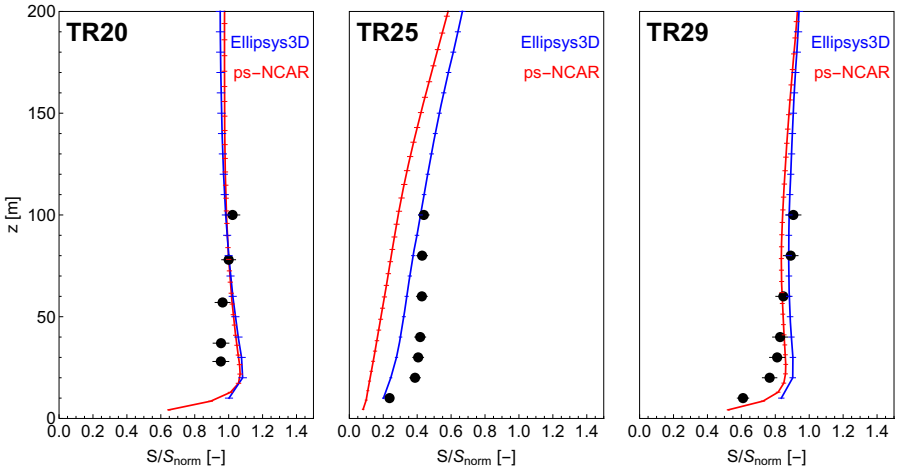

Figure 9: Profiles at TR20, TR25 and TR29 for non-dimensionalized wind speed, S/S_{norm}. The measurements are presented by black dots. All error bars are estimated as standard deviation of the mean, $\sigma/\sqrt{N}$.

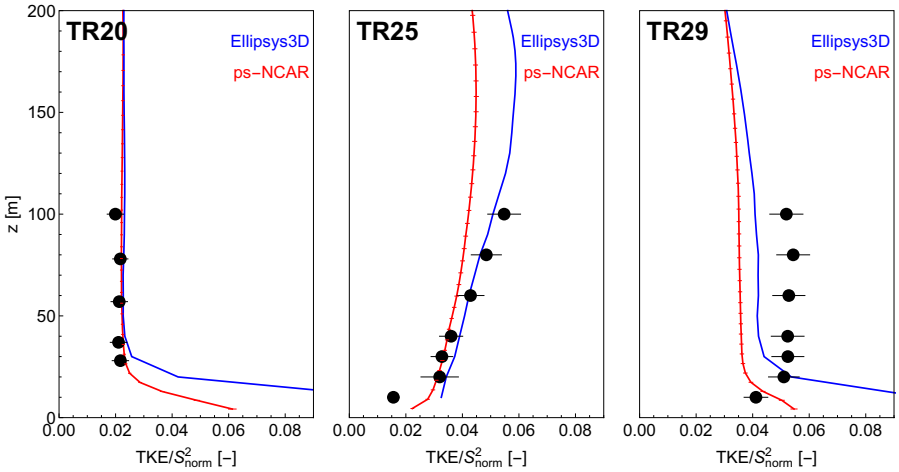

Figure 10: Same as Figure 9 but for non-dimensionalized turbulent kinetic energy TKE/S^2_{norm}.

in Figure 1. Measurements have been selected based on wind direction ($235 \pm 10°$ in 80 m height above terrain at TR20), wind speed ($S > 8\,\mathrm{m\ s^{-1}}$ in 80 m height above terrain at TR20) and stratification (Obukhov length, $|L| > 250$ at 20 m height above terrain at TR20). These criteria have been selected in order to get conditions as close to neutral as possible. We use the mean wind speed, S in 80 m height above terrain at TR20 as the normalization wind, S_{norm}, and hence scale all units of velocity with S_{norm} in order to compare measurements and LES simulations. For the measurements $S_{norm} = 9.15\,\mathrm{m\ s^{-1}}$ and for the simulations, $S_{norm} = 5.3\,\mathrm{m\ s^{-1}}$, and hence some effects on the results from difference in Reynolds number cannot be ruled out, although the effect will most likely be small [7].

We present profiles of 30-min averaged speed, S, in Figure 9. At TR20 (located on the first ridge) the simulations show too high speed close to the surface compared with measurements. This behaviour is also observed at the TR29 (located at the second ridge). We speculate that the constant and relatively low roughness length, $z_0 = 0.5\,\mathrm{m}$, used in the simulations can explain

some of this discrepancy: in reality the surface is covered by trees and other roughness elements. At TR29 the wind away from the surface is well captured by EllipSys3D while ps-NCAR produces slightly to low wind speed. At TR25 (located in the valley between the ridges) the simulated speed is lower for all compared heights. This can be explained with the presence of a cross wind along the ridges (V component) present in the measurements $of 3-4\,\mathrm{m\ s^{-1}}$, but not captured in the LES simulations due to the limited terrain with periodic boundary conditions also in the lateral y direction.

We now turn towards the turbulent kinetic energy, TKE presented in Figure 10. Here the profiles at the three mast locations differs slightly as expected from studying the flow along the main transect. At the first ridge both simulations resemble the measured profile. At TR25, however, the profile from EllipSys3D, is very close to the measured profile. However, due to the lack of cross wind in the simulation (V component) , which would most likely increase the production of TKE, the match is probably somewhat fortuitous. At TR29 both simulations lack TKE for all heights.

It is important to mention that the suite of LES simulations in no way was designed for comparison with the measured profiles. The biggest source of uncertainty we attribute to the limited spatial domain in our simulations and the too simple roughness/land-use description. The resolution used is also rather crude. Even at 40 m we have a very large part of the TKE produces by the SGS model. Also the wind direction is not constant in the measurements [5] and effects from stratification, Coriolis force and other larger scale effects are lacking. Future studies will look at the effect on the flow from changing these.

4. Final remarks

We have performed a detailed comparison between two LES models with different discretization while keeping as many parameters as possible constant. In general we observe very good agreement between the analyzed flow statistics from the two codes. We attribute this to the matureness and robustness of the LES codes and their ability to successfully simulate flow in complex terrain in the atmospheric boundary layer.

We found a 19% increase in the wind speed, U_{norm}, in the simulations with the smoothed terrain compared to using the steep and realistically represented terrain. For wind resource estimations this would have dramatic consequences, and hence the importance of using correct maps can not be underestimated.

We also compared with measured data and found good agreement in wind speed away from the surface on the second ridge and of TKE on the first ridge. On the other hand we also found discrepancy, especially in the valley between the ridges and close to the surface. This was expected due to the simplicity of our setup. We mentioned limited domain, land usage, resolution effects, lack of stratification and Coriolis force, meso-scale effects and non constant wind forcing as possible causes for this. In future work we will try to address these effects one-by-one in order to not only quantify its primary effect upon the flow but also possible secondary non-linear effects.

As more data from the field experiment is being analysed more in-depths validation cases can be constructed which focusses on more specific formulations in the LES codes.

References

[1] A. Bechmann, N. N. Sørensen, J. Berg, J. Mann, and P.-E. Rethore. The Bolund Experiment, Part II: Blind Comparison of Microscale Flow Models. *Boundary-Layer Meteorol.*, 141:245, 2011.

[2] J. Berg, J. Mann, A. Bechmann, M. S. Courtney, and H. E. Jørgensen. The Bolund Experiment, Part I: Flow Over a Steep, Three-Dimensional Hill. *Boundary-Layer Meteorol.*, 141:219, 2011.

[3] J. Berg, N. Troldborg, N.N. Sørensen, E. G. Patton, and P. P. Sullivan. Large-eddy simulation of turbine wake in complex terrain. *Journal of Physics: Conference Series*, 854(1):012003, 2017.

[4] M. Diebold, C. Higgins, J. Fang, A. Bechmann, and M. B. Parlange. Flow over Hills: A Large-Eddy Simulation of the Bolund Case. *Boundary-Layer Meteorol.*, 148(1):177–194, 2013.
[5] A R Meyer Forsting, A Bechmann, and N Troldborg. A numerical study on the flow upstream of a wind turbine in complex terrain. *Journal of Physics: Conference Series*, 753:032041, 2016.
[6] P. S. Jackson and J. C. R. Hunt. Turbulent wind flow over a low hill. *Q. J. R. Meteorol. Soc.*, 101:929, 1975.
[7] R. Kilpatrick, H. Hangan, K. Siddiqui, D. Parvu, J. Lange, J. Mann, and J. Berg. Effect of reynolds number and inflow parameters on mean and turbulent flow over complex topography. *Wind Energy Science*, 1:237–254, 2016.
[8] J. Lange, J. Mann, N. Angelou, J. Berg, M. Sjöholm, and T. Mikkelsen. Variations of the Wake Height over the Bolund Escarpment Measured by a Scanning Lidar. *Boundary-Layer Meteorol.*, 159(1):147–159, 2016.
[9] J. Lange, J. Mann, J. Berg, D. Parvu, R. Kilpatrick, Adrian Costache, J. Chowdhury, K. Siddiqui, and H. Hangan. For wind turbines in complex terrain, the devil is in the detail. *Environ. Res. Lett.*, 12(9), 2017.
[10] J. Mann, N. Angelou, J. Arnqvist, D. Callies, E. Cantero, R. Chávez Arroyo, M. Courtney, J. Cuxart, E. Dellwik, J. Gottschall, S. Ivanell, P. Kühn, G. Lea, J. C. Matos, J. M. L. M. Palma, L. Pauscher, A. Peña, J. Sanz Rodrigo, S. Söderberg, N. Vasiljevic, and C. Veiga Rodrigues. Complex terrain experiments in the new european wind atlas. *Philosophical Transactions of the Royal Society of London A: Mathematical, Physical and Engineering Sciences*, 375(2091), 2017.
[11] J.A. Michelsen. Basis3D - a platform for development of multiblock PDE solvers. Technical report AFM 92-05, Technical University of Denmark, Lyngby, 1992.
[12] J.A. Michelsen. Block structured multigrid solution of 2D and 3D elliptic PDEs. Technical Report AFM 94-06, Technical University of Denmark, 1994.
[13] C.-H. Moeng. A large-eddy-simulation model for the study of planetary boundary-layer turbulence. *Journal of the Atmospheric Sciences*, 41(13):2052–2062, 1984.
[14] W. Munters, C. Meneveau, and J. Meyers. Shifted periodic boundary conditions for simulations of wall-bounded turbulent flows. *Phys. Fluids*, 28(2), 2016.
[15] W. Munters, C. Meneveau, and J. Meyers. Turbulent Inflow Precursor Method with Time-Varying Direction for Large-Eddy Simulations and Applications to Wind Farms. *Boundary-Layer Meteorol.*, 159(2):305–328, 2016.
[16] S. V. Patankar and D. B. Spalding. A calculation procedure for heat, mass and momentum transfer in three-dimensional parabolic flows. *Int. J. Heat Mass Transfer*, 15:1787–1972, 1972.
[17] N. N. Sørensen. General Purpose Flow Solver Applied to Flow over Hills. PhD thesis Risø–R–864(EN), Risø National Laboratory, 1995.
[18] N.N. Sørensen. HypGrid2D a 2-D mesh generator. Technical Report Risø-R1035(EN), Technical University of Denmark, 1998.
[19] R. J.A.M. Stevens, J. Graham, and C. Meneveau. A concurrent precursor inflow method for Large Eddy Simulations and applications to finite length wind farms. *Renew. Energy*, 68:46–50, 2014.
[20] P. P. Sullivan, J. C. McWilliams, and Chin-Hoh Moeng. A subgrid-scale model for large-eddy simulation of planetary boundary-layer flows. *Boundary-Layer Meteorol.*, 71:247–276, 1994.
[21] P. P. Sullivan, J. C. McWilliams, and E. G. Patton. Large eddy simulation of marine atmospheric boundary layers above a spectrum of moving waves. *J. Atmos. Sci.*, 71:4001–4027, 2014.
[22] P. P. Sullivan and E. G. Patton. The effect of mesh resolution on convective boundary layer statistics and structures generated by large-eddy simulation. *J. Atmos. Sci.*, 68:2395–2415, 2011.
[23] P.P. Sullivan, E.G. Patton, and K.W. Ayotte. Turbulent flow over and around sinusoidal bumps, hills, gaps and craters derived from large eddy simulations. In *19th Conference on Boundary Layer and Turbulence, Keystone, CO*, 2010.
[24] P.A. Taylor and H. W. Teunissen. ASKERVEIN '82: Report on the September/October 1982 Experiment to Study Boundary-Layer Flow over Askervein, South Uist. *Atmos. Environ. Service, Downsview, Ontario*, Technical Report MSRB-83-8, 1983.
[25] I. Troen and E. L. Petersen. *European Wind Atlas*. Risø National Laboratory, Roskilde, Denmark, 656 pp, 1989.
[26] N. Vasiljević, J. M. L. M. Palma, N. Angelou, J. Carlos Matos, R. Menke, G. Lea, J. Mann, M. Courtney, L. Frölen Ribeiro, and V. M. M. G. C. Gomes. Perdigão 2015: methodology for atmospheric multi-doppler lidar experiments. *Atmospheric Measurement Techniques*, 10:3463–3483, 2017.
[27] J. L. Walmsley and P. A. Taylor. Boundary-layer flow over topography: Impacts of the Askervein study. *Boundary-Layer Meteorol.*, 78:291–320, 1996.